NeuroImage 57 (2011) 130–139

Contents lists available at ScienceDirect

NeuroImage

journal homepage: www.elsevier.com/locate/ynimg

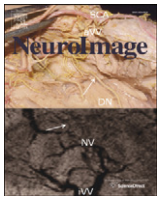

Role of local network oscillations in resting-state functional connectivity

Joana Cabral [a,*,1], Etienne Hugues [a,1], Olaf Sporns [b], Gustavo Deco [a,c]

[a] Theoretical and Computational Neuroscience Group, Center for Brain and Cognition, Universitat Pompeu Fabra, Barcelona 08018, Spain
[b] Department of Psychological and Brain Sciences, Indiana University, Bloomington, IN 47405, USA
[c] Institut Català de Recerca i Estudis Avançats (ICREA), Barcelona, Spain

ARTICLE INFO

Article history:
Received 29 November 2010
Revised 7 March 2011
Accepted 1 April 2011
Available online 12 April 2011

Keywords:
Resting state
Network oscillations
Modeling
Structural connectivity
Functional connectivity
Default-mode network

ABSTRACT

Spatio-temporally organized low-frequency fluctuations (<0.1 Hz), observed in BOLD fMRI signal during rest, suggest the existence of underlying network dynamics that emerge spontaneously from intrinsic brain processes. Furthermore, significant correlations between distinct anatomical regions—or functional connectivity (FC)—have led to the identification of several widely distributed resting-state networks (RSNs). This slow dynamics seems to be highly structured by anatomical connectivity but the mechanism behind it and its relationship with neural activity, particularly in the gamma frequency range, remains largely unknown. Indeed, direct measurements of neuronal activity have revealed similar large-scale correlations, particularly in slow power fluctuations of local field potential gamma frequency range oscillations. To address these questions, we investigated neural dynamics in a large-scale model of the human brain's neural activity. A key ingredient of the model was a structural brain network defined by empirically derived long-range brain connectivity together with the corresponding conduction delays. A neural population, assumed to spontaneously oscillate in the gamma frequency range, was placed at each network node. When these oscillatory units are integrated in the network, they behave as weakly coupled oscillators. The time-delayed interaction between nodes is described by the Kuramoto model of phase oscillators, a biologically-based model of coupled oscillatory systems. For a realistic setting of axonal conduction speed, we show that time-delayed network interaction leads to the emergence of slow neural activity fluctuations, whose patterns correlate significantly with the empirically measured FC. The best agreement of the simulated FC with the empirically measured FC is found for a set of parameters where subsets of nodes tend to synchronize although the network is not globally synchronized. Inside such clusters, the simulated BOLD signal between nodes is found to be correlated, instantiating the empirically observed RSNs. Between clusters, patterns of positive and negative correlations are observed, as described in experimental studies. These results are found to be robust with respect to a biologically plausible range of model parameters. In conclusion, our model suggests how resting-state neural activity can originate from the interplay between the local neural dynamics and the large-scale structure of the brain.

Introduction

In the absence of stimulation or task execution, a mammalian brain exhibits spatio-temporally organized activity. This so-called resting-state activity was initially revealed by slow fluctuations (<0.1 Hz) of the BOLD fMRI signal (Biswal et al., 1995; Gusnard and Raichle, 2001; Greicius et al., 2003; Fox et al., 2005; Raichle and Mintun, 2006; Vincent et al., 2007; Fox and Raichle, 2007). Across voxels from distinct anatomical regions, the BOLD signal was found to be functionally connected, leading to the identification of robust large-scale resting-state networks (RSNs) (Beckmann et al., 2005; Damoiseaux et al., 2006; Mantini et al., 2007). These findings in the BOLD signal have a number of counterparts in neural activity, in particular in the slow power fluctuations of local field potential (LFP) gamma frequency range oscillations (Leopold et al., 2003; Shmuel and Leopold, 2008; Nir et al., 2008; He et al., 2008; Miller et al., 2009; Schölvinck et al., 2010). However, both the link between slow activity and fast gamma oscillations, and the neural mechanisms leading to such spatio-temporally structured activity in different RSNs, remain largely unknown.

We address this problem using a modeling approach. Our main hypothesis is that these phenomena emerge from the interplay between large-scale brain structure and the neural dynamics at the local level. We therefore focus on the large-scale network of long-range structural connectivity (SC) in the brain (connection strengths and conduction delays). At each network node, we assume the existence

* Corresponding author at: DTIC-Universitat Pompeu Fabra, C/ Roc Boronat, 138, 08018 Barcelona, Spain. Fax: +34 93 542 2451.
E-mail address: joana.cabral@upf.edu (J. Cabral).
[1] These authors equally contributed to this work.

1053-8119/$ – see front matter © 2011 Elsevier Inc. All rights reserved.
doi:10.1016/j.neuroimage.2011.04.010

of a network of excitatory and inhibitory neurons whose dynamical state is hypothesized to be above the onset of self-sustained gamma oscillations. In a previous study (Deco et al., 2009), using the macaque's anatomical connectivity (CoCoMac; Kötter, 2004; Kötter and Wanke, 2005) and the dynamically reduced Wilson–Cowan unit model (Wilson and Cowan, 1972) for local node dynamics, this regime of self-sustained oscillations was found capable of reproducing a number of characteristics of resting-state activity. Here, using a similar but simpler oscillator model, we investigate these dynamics in more analytical detail, and we go further by using human cortical SC and comparing our results to empirical functional connectivity (FC) data obtained in earlier empirical studies (Hagmann et al., 2008; Honey et al., 2009). We identify a region of the model parameter space where the simulated FC best matches the empirical FC. In this region, RSNs correspond to partial node clusters with a synchronized oscillatory behavior. Beyond the role of connectivity, we found that delays play an important role in reproducing experimental data.

Methods

Structural connectivity

We use the SC between 66 regions of the human brain (see Fig. 1), downsampled from the high-resolution connection matrix (998 regions of interest (ROIs)) obtained and described in Hagmann et al. (2008), and in Honey et al. (2009). Briefly, following diffusion spectrum and T1-weighted MRI acquisitions, the segmented grey matter was partitioned into 66 anatomical regions according to anatomical landmarks. This was followed by a further parcellation into 998 ROIs. White matter tractography was used to determine which voxel pairs were connected by putative white matter fiber tracts, and to estimate their density and corresponding length, from which the SC was obtained at the ROI level. Since tractography does not give fiber directionality, the connectivity matrix is symmetric at the voxel level. SC was then averaged across 5 subjects. To downsample the SC to 66 regions, the connection strength between two regions was calculated by summing all incoming fiber strengths to the target region, and dividing it by its region-dependent number of ROIs, resulting in a non-symmetric downsampled connectivity matrix. This normalization by the number of ROIs—which have approximately the same surface on the cortex, i.e. the same number of neurons—is required because neuronal activity is sensitive to the number of incoming fibers per neuron in the target region. As the dynamical model of one region already takes into account the effect of its internal connectivity, the connection of a region to itself was set to 0 in the connectivity matrix for the simulations (see Fig. 1B). The length L_{np} of the fiber connecting the region p to the region n was calculated as the average length across all the fibers connecting them. The intra-region length was set to 0 (see Fig. 1C). The region order in these matrices was rearranged according to modules with substantially denser connectivity inside specific node ensembles than with the complementary part of the network. We also took into account the network dynamical behavior in this rearrangement (see Section Network dynamics). Homotopic regions in the two cerebral hemispheres were arranged symmetrically with respect to the matrix center.

Empirical functional connectivity

For the same 5 subjects, the BOLD signal was acquired and preprocessed to obtain the empirical FC at the ROI level, which was then averaged across subjects (see Honey et al. (2009) for details). Briefly,

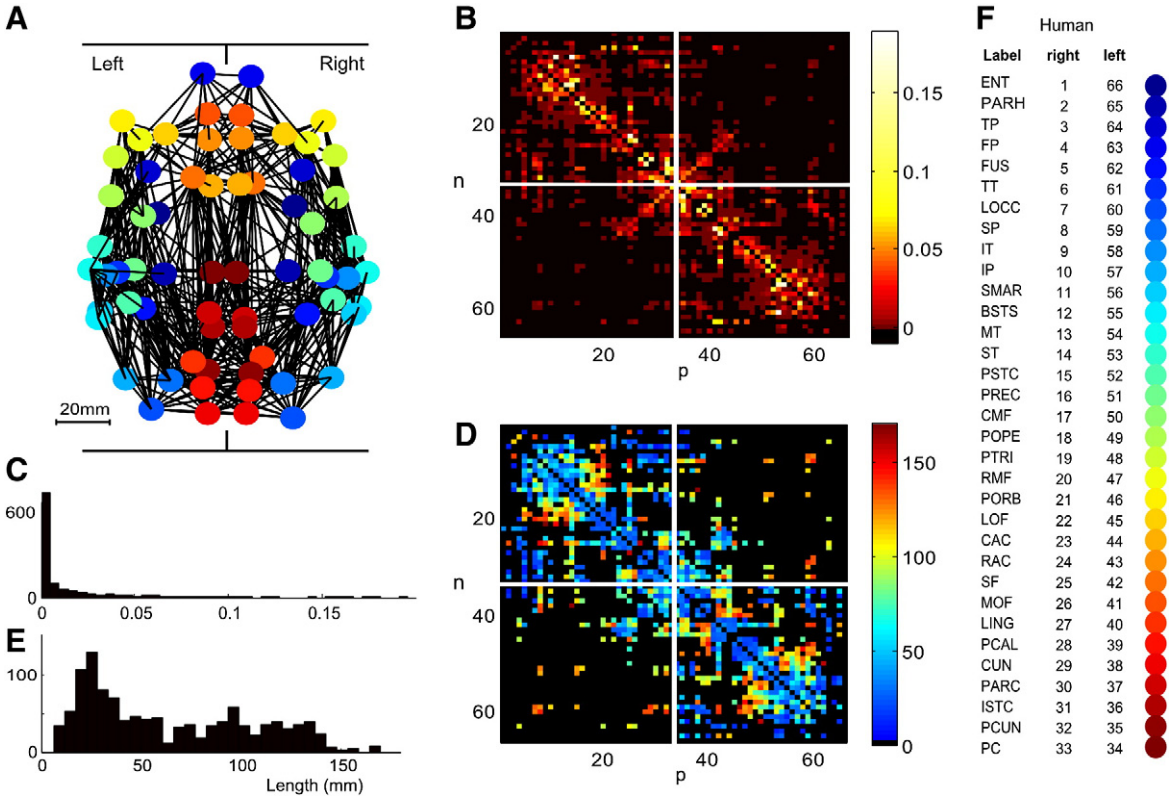

Fig. 1. Structural connectivity of the Human Connectome. A, 2-dimensional representation of the network structure (view from above), the nodes representing anatomical regions placed at their central coordinates. B, Connection strength matrix where n is the source region and p is the target, ordered in a way such that corresponding contra-lateral regions are symmetrically arranged with respect to the matrix centre, the anti-diagonal revealing the existing connections between these contra-lateral regions. The white lines separate the two hemispheres. C, Histogram of the strength of existing couplings. D, Fiber length matrix of existing connections between nodes n and p. The lengths correspond to the average length of all the fibers connecting nodes n and p. E, Histogram of the fiber lengths of existing couplings. F, Cortical regions index: in A the regions are color-coded whereas in C and D the matrix indices indicate the corresponding region.

the BOLD signal was acquired for a total of 20 min (TR = 2 s), while the subjects were resting with eyes closed. A number of preprocessing steps were applied to the BOLD time series (see Honey et al. (2009) for details) including the regression of the global signal (Fox et al., 2005). Then, the correlation matrix was calculated to obtain the FC. The downsampled FC between a pair of regions was obtained as the average of all interregional FC correlations at the ROI level.

Neural dynamics model

We simulated the neural activity on a network of N nodes defined using the previously described SC: the connection strength matrix C (normalized so that the mean strength is 1) and the fiber length matrix L which we transformed into a conduction delay matrix τ by the choice of a conduction velocity. We defined the mean delay $\langle\tau\rangle$ by $\langle\tau\rangle = \langle L\rangle/V$, where $\langle L\rangle$ was the mean fiber length. In the following and for practical reasons, we used the parameter $\langle\tau\rangle$ instead of V.

As observations at the BOLD level have been found to have counterparts in the neural activity, in particular in the slow power fluctuations of the LFP in the gamma frequency range (Leopold et al., 2003; Shmuel and Leopold, 2008; Nir et al., 2008; He et al., 2008; Miller et al., 2009; Schölvinck et al., 2010), we investigate here if locally generated gamma activity can induce correlations at the BOLD level. Each local node represents a neural network of excitatory and inhibitory spiking neurons. As we are interested in the effect of the large-scale SC on neural dynamics, we consider, for simplification, these local networks to have internally homogeneous structure. For numerical tractability, we will represent the network dynamics in a reduced manner, that is, at the neural population level. *In vivo* electrophysiological recordings have shown that neural activity at the population level usually exhibits oscillations with a moderate level of synchrony, in particular in the gamma frequency range (30–80 Hz). In a number of experimental and theoretical studies (Bartos et al., 2007; Brunel, 2000; Brunel and Wang, 2003; Borgers and Kopell, 2003), local neural networks have been shown to exhibit gamma oscillations, and the mechanisms leading to such oscillations are now widely accepted. However, two major dynamical regimes have been found: either the network is in an asynchronous state, where oscillations appear as resonances in the network response and manifest only transiently (Mattia and Del Giudice, 2002; Brunel and Wang, 2003), or the network exhibits self-sustained oscillations (see Borgers and Kopell (2003) for example). Although there is a qualitative difference between these two dynamical regimes,[2] the network could be in one regime or the other when exhibiting a moderate level of synchrony. Following the results from Deco et al. (2009) where the local nodes, modeled as Wilson–Cowan units, exhibited self-sustained oscillations, we assume here that local networks are in this latter regime. In that case, the network intrinsically describes a closed periodic trajectory in phase space, called a limit cycle. When this network receives sufficiently weak inputs, its trajectory is perturbed but remains in the vicinity of this cycle. In this case, it can be shown that the dynamics can be closely approximated by a single dynamical variable: the angle or phase on this cycle. Weak inputs appear as a small perturbation term in the dynamical equation. The resulting node model is a phase oscillator and the network is called a network of phase oscillators (see Fig. 2 for a model illustration). In the same approximation, the influence that one node exerts on another can be written as a 2π-periodic coupling function of the phase difference between the two oscillators, taking into account the interaction delay. Since this function is difficult to evaluate for a neural network, we have chosen its simplest form, the sine function (the first term in the Fourier series). The resulting model is the well studied Kuramoto model (Kuramoto, 1984; Yeung and Strogatz, 1999; Acebrón et al., 2005), which has been used to simulate the behavior of a number of coupled oscillators systems. Denoting by $\theta_n(t)$ the phase of node n at time t, it then obeys the following dynamical equation:

$$\frac{d\theta_n}{dt} = \omega_n + k\sum_{p=1}^{N} C_{np}\sin\left(\theta_p\left(t-\tau_{np}\right)-\theta_n(t)\right) + \eta_n(t), n = 1,\ldots,N.$$

C_{np} is the relative coupling strength from node p to node n, and is the global coupling strength which scales all connection strengths. k must be sufficiently small for two reasons: the above reduction to phase variables must remain valid and, due to moderate local neuronal synchrony, the underlying limit cycles must not be destroyed. The delay τ_{np} between node p and node n is calculated using $\tau_{np} = L_{np}/V = \langle\tau\rangle L_{np}/\langle L\rangle$. The connectivity and the delay matrices are fixed in their structures: only their scaling can be varied with k and $\langle\tau\rangle$, respectively. $f_n = \omega_n/2\pi$ is the intrinsic frequency of node n on its limit cycle, and is drawn from a fixed Gaussian distribution with mean f_0 ($f_0 = 60$ Hz here) and standard deviation σ_f. The terms $\eta_n(t)$, representing the noise received by the local networks, correspond to uncorrelated Gaussian white noise with zero mean ($\langle\eta_n(t)\rangle = 0$) and variance σ_n^2/T ($\langle\eta_n(t)\eta_p(s)\rangle = \delta_{np}\delta(t-s)\sigma_n^2/T$), where δ_{np} is the Kronecker delta, $\delta(.)$ is the Dirac delta function, σ_n is in radians and T is a given timescale ($T = 1$ s here). Frequency dispersion and noise, both naturally present in the brain, have been considered in the model for realism, and we will study the robustness of our conclusions with regard to these parameters.

The present model depends on 4 main free parameters: $\langle\tau\rangle$, k, σ_f and σ_n. After an extensive numerical exploration of this parameter space, we have found the main free parameters to be the mean delay $\langle\tau\rangle$ and the global coupling strength k, for which we have performed

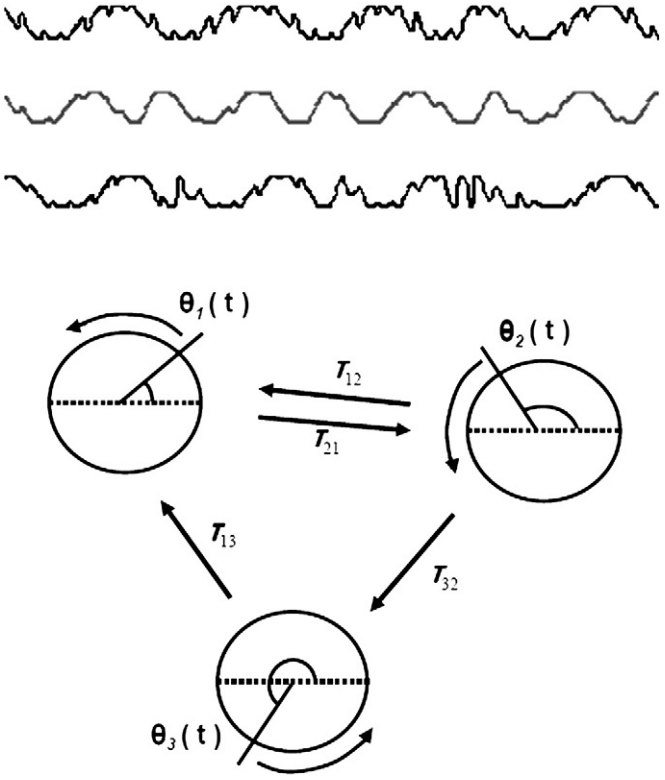

Fig. 2. Graphical representation of the model. (top) Example of 3 time series obtained from $r_n(t) = \sin(\theta_n(t))$; (bottom) a set of 3 inter-connected phase oscillators, with delayed interactions τ_{np}, where the angle on the circle represents the phase on the limit cycle of self-sustained neuronal oscillations.

[2] In dynamical systems language, a bifurcation separates these two regimes. The position of this bifurcation depends on conditions or parameters, such as the strength of the external stimulation.

an exhaustive parametric study. For biological realism, we also considered the effect of σ_f and σ_n but, due to their relatively small influence on the behavior of the network in their respective plausible range compared to the 2 other parameters, and due to the high cost of simulating the complete 4 dimensional parameter space, we conducted only a partial parametric study: the influence of large values of these two parameters in the results across the ($\langle\tau\rangle$, k) plane, and how these parameters influence the results for the chosen working point ($\langle\tau\rangle$, k) = (11, 18) (see Supplementary Figs. 2–5).

Phases were initialized randomly. Furthermore, due to delays, we had to specify the phases for a sufficiently long interval and we did that as in a non-interacting (and non-noisy) network. We always discarded the first simulated 20 s to avoid our results being dependent on initial conditions and we always refer to the remaining simulated time in the following. When exploring the parameter space ($\langle\tau\rangle$, k), we simulated the previous system for 300 s. To compare with experimental FC, we simulated for 1200 s (20 min) for the chosen ($\langle\tau\rangle$, k) pair. The system of N dynamical equations was numerically integrated with a time-step $\Delta t = 0.1$ ms using an Euler scheme adapted to noise (Platen, 1999)). All calculations were performed using MATLAB (http://www.mathworks.com).

At the global level, the network synchrony can be evaluated by the order parameters $R(t)$ and $\Phi(t)$, jointly defined by

$$R(t)e^{i\Phi(t)} = \frac{1}{N}\sum_{n=1}^{N} e^{i\theta_n(t)}.$$

$R(t)$ measures phase uniformity and varies between 0 for a fully desynchronized—or incoherent—state to 1 for a fully synchronized state. For sufficient synchrony, $\Phi(t)$ describes the movement of the oscillator ensemble around the unit circle. We characterize the network dynamics by the mean synchronization level $\overline{R}$ and the standard deviation σ_R of the order parameter $R(t)$ over the simulated time interval. $\overline{R}$ is an index of the global synchronization level while σ_R indicates the level of metastability of the network (Shanahan, 2010).

For particular clusters of nodes (see Section Network dynamics), we calculated the order parameters $R_c(t)$ and $\Phi_c(t)$ defined accordingly, where the sum is now performed for nodes belonging to a cluster c.

Simulated BOLD and functional connectivity

To relate the simulated local neural activity to the BOLD signal, we used the Balloon-Windkessel hemodynamic model (Friston et al., 2003). For the neurovascular coupling we built on the assumption that the physical quantity whose variations underlie BOLD signal was the firing rate of the local neuronal population, which is the basic quantity associated to the phase model. In the model, the firing rate—$r_n(t)$ for node n—fluctuates around a fixed value and these fluctuations are given by a periodic function of the local node phase. As we do not know this function, we have made the simple choice of the sine function, that is $r_n(t) = r_0 \sin(\theta_n(t))$. By definition of the local phase oscillator model, these fluctuations have a fixed amplitude r_0. In the simulations, we have considered relatively small amplitude ($r_0 = 1$) so that the Balloon–Windkessel model is linear and is analogue to a linear filter (see Supplementary Fig. 1). In doing so, we prove that our results depend only on the neural activity generated by the model, and not on the non-linearities of the BOLD model.

Note that, using more biophysical and/or neural mass models, a number of neurovascular couplings have been considered in the literature (Kilner et al., 2005; Rosa et al., 2010; Friston et al., 2010). However, due to the simplicity of our model where local dynamics is described by a single variable, fundamentally the firing rate, we have to rely on this variable. However, as we will show later, since the origin for BOLD correlations between nodes relies on their synchrony—or in other words their identity, any variable derived from the rate as input to the BOLD model would have essentially given the same conclusions.

To understand why the BOLD signal is generally correlated for nodes inside the same cluster, as long as it is sufficiently synchronized, we need to decompose the neural activity using the following identity

$$e^{i\theta_n(t)} = R_c e^{i\Phi_c(t)} + e^{i\Phi_c(t)}\left[e^{i\Delta\theta_n(t)} - R_c(t)\right] \quad (1)$$

where $\Delta\theta_n(t) = \theta_n(t) - \Phi_c(t)$ is the relative angle of the node inside its cluster, and we then took the imaginary part to recover $r_n(t)$. The more the cluster is synchronized, the more the absolute value of the first term tends towards 1, and the more the absolute value of the second tends towards 0. Therefore, when the cluster synchrony is sufficiently high, the first term in Eq. (1), which is common for all cluster nodes and is an intrinsic characteristic of the cluster, increases its value relatively to the second one, and the dynamics of different nodes inside the same cluster becomes correlated. The same happens for the low-pass filtered (<0.35 Hz) dynamics, which is strongly correlated to the BOLD signal (see Figs. 1C–D in Supplementary Material). Therefore, BOLD signals get correlated inside a cluster when it is sufficiently synchronized.

To compare the model results with the empirical FC, we low-pass filtered (<0.25 Hz) and downsampled the BOLD time series at 2 s to achieve the same resolution as in Honey et al. (2009). The low-pass filtering eliminates small and non-physiological high frequency components in the BOLD signal that can induce spurious correlations. Finally, the simulated FC was obtained after regressing the global signal (average over all regions) out of the regional BOLD time series (Fox et al., 2005, 2009), and by computing the correlation matrix. To compare the simulated and the empirical FCs, we calculated the Pearson correlation and the distance between the two matrices only for the structurally connected pairs (to increase the effectiveness of these measures; see Supplementary Fig. 6). Later, for the chosen working point, we used a seed approach and compared the two matrices row by row, calculating the Pearson correlation coefficient between rows, and the corresponding p-value. This gives the probability of getting a correlation as large as the observed one when the true correlation is zero. The correlation is significant when $p < 0.05$.

For clarity, all methods used in this paper are summarized in a flowchart shown in Fig. 3.

Results

Structural connectivity

We consider the network dynamics supported by the SC of the human brain (Hagmann et al., 2007, 2008) (see Section Structural connectivity). A geometrical view from above of the considered network is represented in Fig. 1A. The connectivity strength matrix together with the fiber length matrix is shown in Figs. 1B and C, respectively. For each region, the abbreviations corresponding to the indices are indicated in Fig. 1F (see Supplementary Table 1 for the complete list of brain regions). The distribution of strength values decreases sharply (see Fig. 1D) and the fiber length distribution exhibits a somewhat bimodal shape (see Fig. 1E). Confirming previous observations about the small-world structure of brain networks (Bullmore and Sporns, 2009), the region reordering (see Section Structural connectivity) revealed a complex community structure of the adjacency matrix. It specifically unveiled the presence of node clusters, which are much more connected inside than outside the cluster to which they belong. As we will demonstrate below, this non-randomness of adjacency matrices together with fiber strength and length, have consequences on the dynamics.

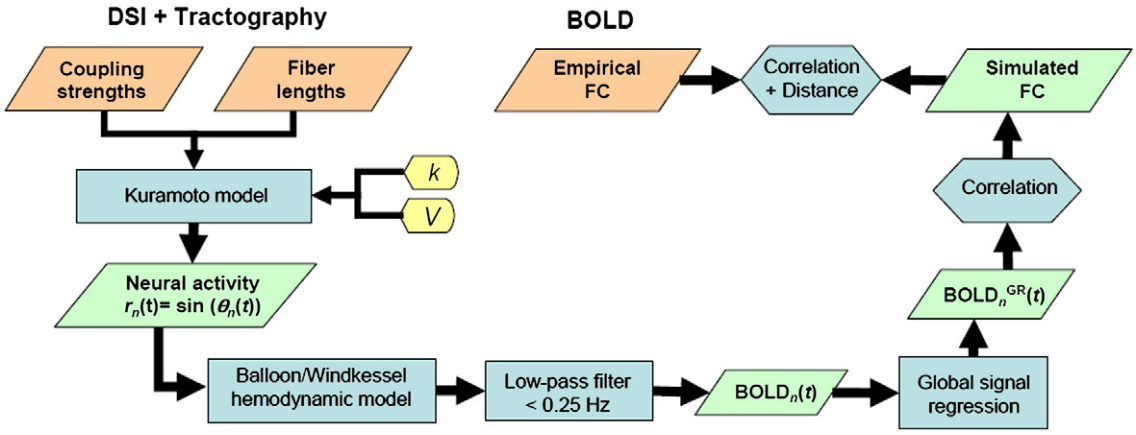

Fig. 3. Flowchart illustrating all the methods employed here to go from the empirical SC to the simulated FC, as explained in Methods. (Orange) experimental inputs, (green) simulated data, (blue) processes, and (yellow) free parameters.

Network dynamics

The matrices of connection strengths and fiber lengths are given by the human SC considered here. After a thorough numerical exploration of the 4-dimensional parameter space for the biologically plausible range of values for σ_n and σ_f, and taking into account the theoretical results about the behavior of the Kuramoto model, we have found that the model exhibits the highest sensitivity to the ($\langle\tau\rangle$, k) plane. To understand the role of each parameter, we report here the exploration of this plane using $(\sigma_n, \sigma_f) = (0, 0)$, $(0, 3)$, $(2, 0)$ and $(2, 3)$. We also explore the effects of σ_n and σ_f in their respective range for the working point we finally choose in the ($\langle\tau\rangle$, k) plane.

The behavior of the Kuramoto model has been described theoretically essentially as a function of the global coupling strength k (Acebrón et al., 2005). For large N, the global coupling exhibits a critical value k_c for which the network exhibits a synchronization transition between an incoherent motion of the oscillators ($k<k_c$) and partial synchrony ($k>k_c$). This transition is described by the order parameter R that measures the network synchrony level. It jumps from zero, below k_c, to a positive value, above. For small N , i.e. for a finite-size network, R is usually never null, and there is a similar but smoother transition in the behavior of R as a function of k. In the following, the region below the critical coupling will be called the incoherent region.

In (Lee et al., 2009), the case of a delay distribution (in particular, a gamma distribution) was addressed theoretically for an infinite network with homogeneous coupling. In that case, the critical coupling $k_c(\langle\tau\rangle)$ was found to be an increasing function when the delay distribution was sufficiently large compared to its mean, meaning that synchrony requires higher coupling as the mean delay increases.

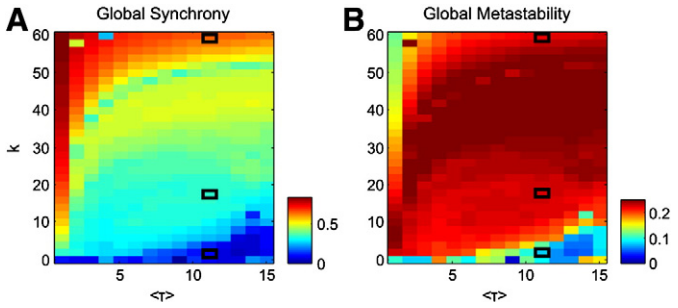

Fig. 4. Global dynamics in the mean delay and global coupling parameter space. A, Global level of synchrony measured as the mean of the order parameter $\bar{R}$. B, Standard deviation of the order parameter σ_R. The dynamics of the points highlighted with black rectangles are shown in Fig. 5.

Despite high heterogeneity of the finite-size human SC observed here, the smoother transition towards synchrony draws a line of similar shape (see Fig. 4A). In particular, for sufficiently small delays, the network synchronizes even for a very weak coupling. Similarly to the theoretical case, as the mean delay increases, synchrony fades away, and the network needs increasingly higher coupling to synchronize.

In general, a network state, as described by the order parameter $R(t)$, is never found to be stationary, with all oscillators always having the same frequency. There is a continuous relative movement between oscillators, which manifests itself in the standard deviation σ_R of the order parameter $R(t)$, as shown in Fig. 4B. For sufficiently large coupling but below the synchronization transition, $R(t)$ exhibits large fluctuations (as illustrated in Fig. 5A middle) and the standard deviation σ_R is the highest. The dynamics is the most irregular in this region, similarly to what has been found for a finite-size Kuramoto network with full connectivity and no delays (Popovych et al., 2005).

Due to the heterogeneous connectivity of the SC (see Methods 2.1 and Fig. 1), in this intermediate region, subsets of nodes—that we will name clusters in the following—exhibit a high level of synchrony while the global synchrony value is still low (see Fig. 5 middle). This represents an intermediate regime between incoherence and global synchronization. For this reason, the transition to synchrony was found to be less abrupt than for homogeneously or randomly coupled networks as predicted by theory (data not shown). In this region, the nodes of a cluster are entrained by the cluster but still move relative to it, explaining the temporal fluctuations of the cluster synchrony levels (see Fig. 5 middle). As coupling increases, clusters progressively merge to form bigger clusters, finally merging into a single one (see Fig. 5 right).

Even if network oscillations in the same frequency band are observed across brain areas, usually there is some discrepancy in their peak frequency. For the gamma band considered here, we modeled the dispersion of frequencies around 60 Hz as a Gaussian distribution, such that $\sigma_f<5$ Hz. When we consider noise, we limit ourselves to $\sigma_n<3$ rad so that noise-induced fluctuations are sufficiently weak so as not to perturb too strongly the dynamics around the limit cycle. In their plausible range, both frequency dispersion and noise, either considered separately or simultaneously, are found to have a small effect on the dynamics. Indeed, the qualitative features of the dynamics are preserved, such as the formation of clusters for sufficient mean delay and intermediate coupling. Moreover, the mean and the fluctuations of the order parameter behave very similarly to the case where $(\sigma_n, \sigma_f) = (0, 0)$ in the whole ($\langle\tau\rangle$, k) plane (see Supplementary Fig. 2). Particularly, the regions of small mean delay or high coupling still exhibit synchrony. In the parameter space region where individual clusters or the whole network synchronize, the robustness of

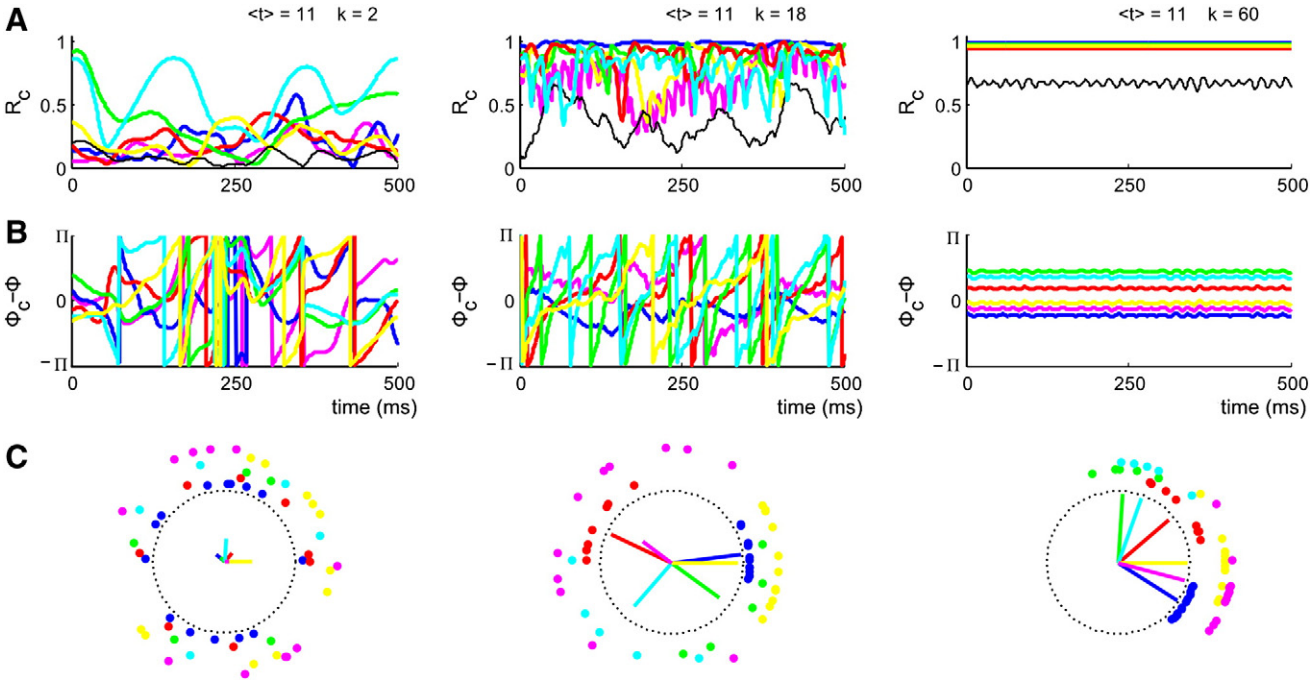

Fig. 5. Cluster dynamics for $k=2$ (left), 18 (middle) and 60 (right), with $\langle\tau\rangle=11$ m (highlighted in Fig. 4). *A*, Global synchrony level $R(t)$ (black) and cluster synchrony level $R_c(t)$ (each color represents a subset of nodes, corresponding to a cluster seen at $k=18$) as a function of time. *B*, Cluster phase $\Phi_c(t)$ relative to the global network phase $\Phi(t)$ as a function of time. *C*, Snapshot of node phases at $t=250$ ms (nodes have the color of the cluster to which they belong). Inside the circle and for each cluster, we represent the corresponding order parameter using a vector whose length is $R_c(t)$ and phase $\Phi_c(t)$. As k increases, clusters go progressively from incoherence (left) to cluster synchrony (middle) until reaching global synchrony (right).

the dynamics to frequency dispersion or noise perturbations is due to the fact that nodes are attracted towards a cluster or the network, respectively. Overall, these results show that the spatiotemporal organization of the network dynamics is quite robust to the local dynamics characteristics and reinforce the importance of SC in the dynamical organization of the network.

Resting-state functional connectivity

The fMRI BOLD signal is intrinsically a low-frequency signal due to the temporal scale of the hemodynamic response function. Similarly, the Balloon/Windkessel model of Friston et al. (2003), which estimates the BOLD signal from a given neural activity, gives a low-frequency BOLD signal (see Section Simulated BOLD and functional connectivityfor the subsequent filtering of non-biological residual fast fluctuations). The model first calculates the blood flow using a low-pass filter up to approximately 0.5 Hz (see Supplementary Fig. 1A) before calculating the BOLD signal using a nonlinear model. The blood flow fluctuations are therefore proportional to the neural activity amplitude r_0. For the amplitude we have used in the simulations ($r_0=1$), we have verified that the blood flow fluctuations remain relatively small (see Supplementary Fig. 1B), so that the Balloon/Windkessel model behaves as a linear filter. Consequently, our results at the BOLD level are not linked to non-linearities of the BOLD model but emerge from the properties of the neural activity. The low-pass filtered (<0.35 Hz) simulated neural activity correlates strongly ($r=0.88$) with the corresponding simulated BOLD signal, with a lag corresponding to the time-to-peak of the correlation function (see Supplementary Figs. 1C–D). Therefore, finding correlations in the BOLD signal is similar to finding these correlations in the slow fluctuations of the neural activity. In the regions of the $(\langle\tau\rangle, k)$ plane where the network synchronizes or is fully incoherent, the dynamics is too regular and fast, and therefore the BOLD signal has a small amplitude and power. On the other hand, in the intermediate region, the irregularity of the neural activity creates significant power at low frequency and consequently in the BOLD signal.

To identify the region of the parameter space where the model best reproduces the empirical FC, we computed the Pearson correlation and the distance between the empirical and the simulated FC matrices (see Fig. 6A). Both indicators are complementary as each has its own limitations. In doing so, we only took into account the FC for directly connected pairs of regions since these were essentially the ones that varied substantially across the parameter space (See Section Simulated BOLD and functional connectivity and Supplementary Fig. 6). The region of simultaneous large correlation and small distance corresponds to a subregion of the incoherent region where dynamical clusters of nodes appear. It coincides with a mean delay between 9 and 14 ms. For a given point in this region, the correlation matrix of neural activity (see Fig. 6B left, where $(\langle\tau\rangle, k)=(11, 18)$) clearly exhibits blocks of large positive correlation, revealing the existence of synchronized clusters. When comparing with the BOLD correlation matrix (see Fig. 6B right) we see that the BOLD signal can be correlated between the nodes of a cluster. However, cluster synchrony is not sufficient to induce BOLD correlation: this is the case only when synchrony is sufficiently high and nodes follow tightly the cluster movement.

Why is the agreement between simulated and empirical FC best in the region where clusters form? The highest empirical correlations correspond mainly to pairs linked by direct SC (Honey et al., 2009). The best agreement occurs when the simulated correlation is also high for these pairs. In Fig. 6C, we have plotted the correlation between the low-pass filtered (<0.35 Hz) node dynamics and the cluster dynamics to which a node belongs (using the first term in the right hand side of Eq. (1)). As k increases (from left to right), clusters synchronize, and the slow dynamics of nodes in the same clusters—and therefore BOLD signals—become correlated. Finally, since a substantial part of the connected pairs of regions are located in the same clusters, this explains the best agreement with empirical FC in this region.

At the network dynamics level, FC remains remarkably stable when frequency dispersion and noise are considered. This is true over the $(\langle\tau\rangle, k)$ plane, except in the region of high synchrony corresponding to small delays or high coupling when noise is considered (see

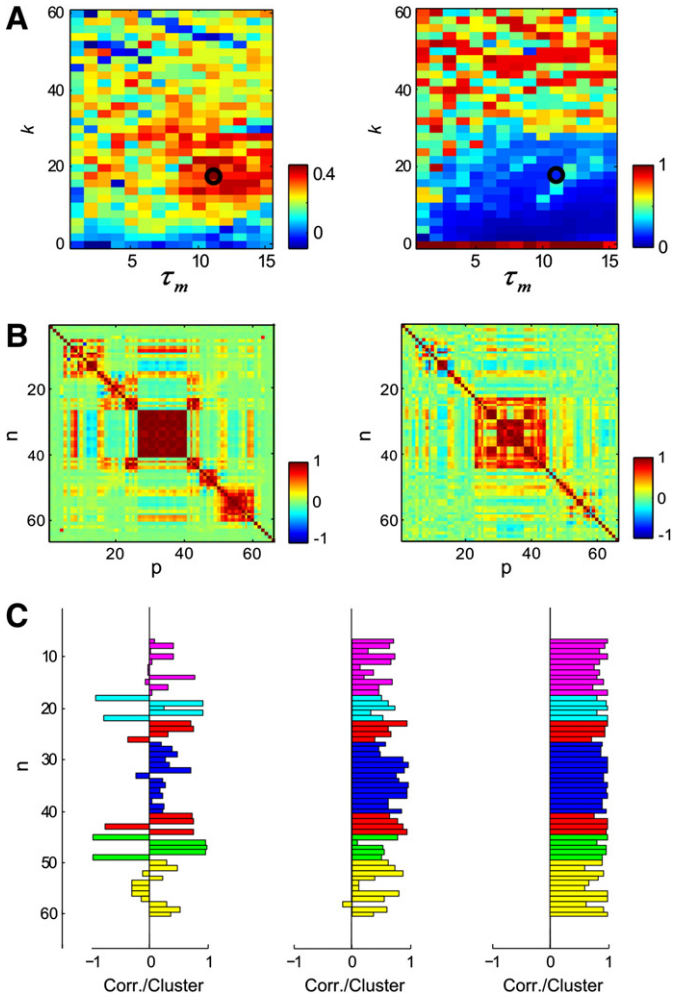

Fig. 6. Behavior of the simulated FC in the parameter space. A, Pearson correlation (left) and mean squared error (right) between the empirical and the simulated FC in the whole parameter space considering only the connected pairs of regions. These results reveal an extended region (in red in the left plot) of large delay and intermediate coupling in the incoherence region of the parameter space where the agreement is the best (maximal correlation and minimal error). B, (left) Correlation matrix of the simulated neural activity and (right) correlation matrix of the corresponding BOLD signal for the selected working point $(\langle\tau\rangle, k) = (11, 18)$ (black circle in A). C, Correlation between the low-pass filtered (<0.35 Hz) node dynamics and cluster dynamics to which a node belongs (using the first term in the right hand side of Eq. (1)), for k = 2 (left), 18 (middle) and 60 (right). As the cluster synchrony level increases, the slow dynamics of its nodes becomes correlated due to the correlation that each node dynamics acquire with the cluster to which it belongs.

Supplementary Fig. 3), where the simulations predict empirical FC up to a certain degree, although not as well as in the region of realistic delays. The reason is that noise destroys high BOLD correlations between many nodes, especially between the clusters seen in the intermediate region (data not shown). However, even with noise, this region is not appropriate because the global synchrony of the oscillatory dynamics contradicts experimental data. For the chosen working point, the FC obtained, with or without frequency dispersion and noise, remains very stable (see Supplementary Fig. 4). Interestingly, noise seems to eliminate much of the perturbations induced on the FC by frequency dispersion (see 2nd and 4th columns of Supplementary Fig. 4). To further examine the influence of these parameters, we have looked at their separate effects by varying them continuously for the chosen working point (see Supplementary Fig. 5). In their respective biologically plausible range (σ_f<5 Hz and σ_n<3 rad), the high correlation and low distance with the empirical FC is essentially maintained.

In the center of the region of best agreement with empirical FC, i.e. the region where synchronized clusters appear, we have selected the working point $\langle\tau\rangle = 11$ ms and $k = 18$. This corresponds to a transmission speed of 6 m/s, which is in the physiologically realistic range of propagation velocities (around 5–20 m/s) for the adult primate brain according to Ghosh et al. (2008a). For increased biological realism, we added noise with $\sigma_n = 1.25$ rad. A detailed comparison between the simulated and the empirical FC for this working point is presented in Fig. 7. In Figs. 7A–B, we present the SC, the empirical FC and the simulated FC with all other network regions for three seeds, two from the Default-Mode Network (DMN), the right precuneus (rPCUN) in Fig. 7A (top) and the left posterior cingulate cortex (lPC) in Fig. 7B, and one from a distinct network, the left cuneus (lCUN) in Fig. 7A (bottom). In Fig. 7C, we can see that the correspondence between seed maps, given by the Pearson correlation between simulated and empirical FCs for a given seed, is significantly high for all seeds. As previously reported in Honey et al. (2009) we see that, in general, FC is positively correlated with SC for directly connected node pairs. Furthermore, the simulations predict many of details in the pattern of the empirical FC between DMN regions along the medial axis. On the other hand, correlation maps of more distant seeds are less well predicted (see Supplementary Fig. 6). It is important to mention that, beyond the model quality—i.e. the way the dynamics at the local node level is modeled—results also depend crucially on the quality of the SC matrix. Some fiber tracts, for example long inter-hemispheric connections between lateral cortices, are likely missing due to the limited resolution of current imaging techniques (Hagmann et al., 2008). These missed pathways have direct repercussions on the model results. Also, the fact that empirical FC has smaller values than the simulated one is due in part to the effect of averaging while down-sampling the high-resolution empirical FC.

Regarding the patterns of correlations outside clusters, an analysis of the model dynamics is difficult to obtain, since different clusters seem to interact in a non-trivial way (see Fig. 5B middle). From this, it is difficult to infer if two different clusters will lead to correlated or anti-correlated BOLD signals. However, a comparison between patterns of correlations in the empirical and simulated FC can be done. In Fig. 8 we checked if the model could reproduce anti-correlated networks as observed in Fox et al. (2005). Indeed, the lPC seed exhibits positive correlation (r = 0.5) with the left superior frontal (lSF), and negative correlation (r = −0.3) with the left lateral occipital cortex (lLOCC) in the model. This result agrees with the empirical measures. In particular, these correlations can be seen directly in the simulated BOLD signal time series of the 3 seeds (Fig. 8 bottom).

Discussion

In this study, we propose a large-scale neural network model to explain the origin of spatiotemporal patterns of slow fluctuations observed in the BOLD signal during rest, in other words the RSNs. As BOLD observations have been found to have counterparts in the neural activity, in particular in the slow power fluctuations of the LFP in the gamma frequency range (Leopold et al., 2003; Shmuel and Leopold, 2008; Nir et al., 2008; He et al., 2008; Miller et al., 2009; Schölvinck et al., 2010), we investigate here if local gamma activity alone can induce correlations at the BOLD level. *In vivo* electrophysiological studies have reported the existence of oscillations in this frequency band and much experimental and theoretical evidence supports that gamma oscillations are generated at the level of local neuronal populations. In our model, we further assume that each node spontaneously exhibits sustained gamma oscillatory activity. We have used here a simple model—the Kuramoto model—whose behavior has been rather well studied theoretically in simpler parameter settings (Kuramoto, 1984; Yeung and Strogatz, 1999; Acebrón et al., 2005). In the present study, BOLD fluctuations are found to correspond to the

slow part of the neural activity. To constrain the model, we calculated the simulated FC and compared it to the empirical one. After numerically exploring the parameter space, we have identified a region where the simulated FC best matches the empirical one. In this region, delimited by an interval of sufficiently high coupling and realistic transmission delays, partial clusters of well-connected nodes exhibit a significant level of synchrony, while the global network is still in a globally incoherent regime. Inside a cluster, the BOLD signal is correlated between nodes because of the existence of sufficiently strong cluster synchrony. This leads to a shared part of the dynamics between the nodes even if the cluster itself, as characterized by the behavior of its order parameters, has non-stationary dynamics. In this region of intermediate coupling in the incoherence region, we also find irregular dynamics, which induce a wide spectrum in the node dynamics, and is at the origin of the power found at very low frequencies, in particular in the frequency range characteristic of the BOLD signal. Note that this type of dynamical behavior is not surprising for the model considered here, as high-dimensional nonlinear dynamical systems generally exhibit some degree of chaoticity. In this respect, an earlier study of a finite-size Kuramoto model, with full connectivity and without delays, has demonstrated the existence of chaos in the incoherence region (Popovych et al., 2005). Therefore, in the model, the RSNs are instantiated in this region of intermediate coupling and delays by these sufficiently synchronized clusters. Between clusters, we also found patterns of positive and negative correlations that reproduced observed empirical patterns. Although the patterns of FC are largely dependent on the SC, as noticed in the empirical data (Honey et al., 2009; Bullmore and Sporns, 2009), they also emerge from the interplay of SC and local oscillatory dynamics. Beyond the role of the connectivity matrix, the delay matrix was also found to play a major role in preventing the full synchronization of the network. Actually, the network globally synchronizes when the mean delay is too small, even when biologically plausible dispersion of intrinsic frequencies and noise level are considered.

Moreover, the region of best agreement with empirical FC was obtained when the mean delay was above a certain bound (about 9 ms here). All these results were found to be robust to the dispersion of intrinsic frequencies and to noise, both important sources of variability.

The agreement of the model results with the empirical data depends not only on the type of dynamics and on the precise mathematical model that we have considered at the local level, but also on the quality of the SC. Although the empirical FC is related to the actual brain dynamics, errors in the measurement of SC can obscure actual contributions of SC to FC. For example, very few inter-hemispherical connections were detected between regions outside the cortical midline (Fig. 1B). Diffusion imaging and tractography have difficulty detecting actually present structural connections when tracking small fibers perpendicular to major fascicles, and across the corpus callosum. These missing connections may be responsible for the lower agreement between empirical and simulated FC when the seed is not placed in or near to medial cortical regions. Other brain regions not captured in the structural scans (e.g. the thalamus) might also have an important role in shaping FC. Still, despite methodological limitations and using only cortical SC, we have been able to identify a number of important features of the empirical FC.

Previous modeling studies have investigated the brain's neural dynamics during rest and the relationship between SC and FC in this behavioral state, using similar large-scale networks but with more biologically detailed models for the node dynamics. In these cases, all conclusions were based on numerical simulations, and no analytic link to a theoretical understanding of the network dynamics in simple parameter settings (as shown here) was possible. In Ghosh et al. (2008a, 2008b) and Knock et al. (2009), using the CoCoMac database

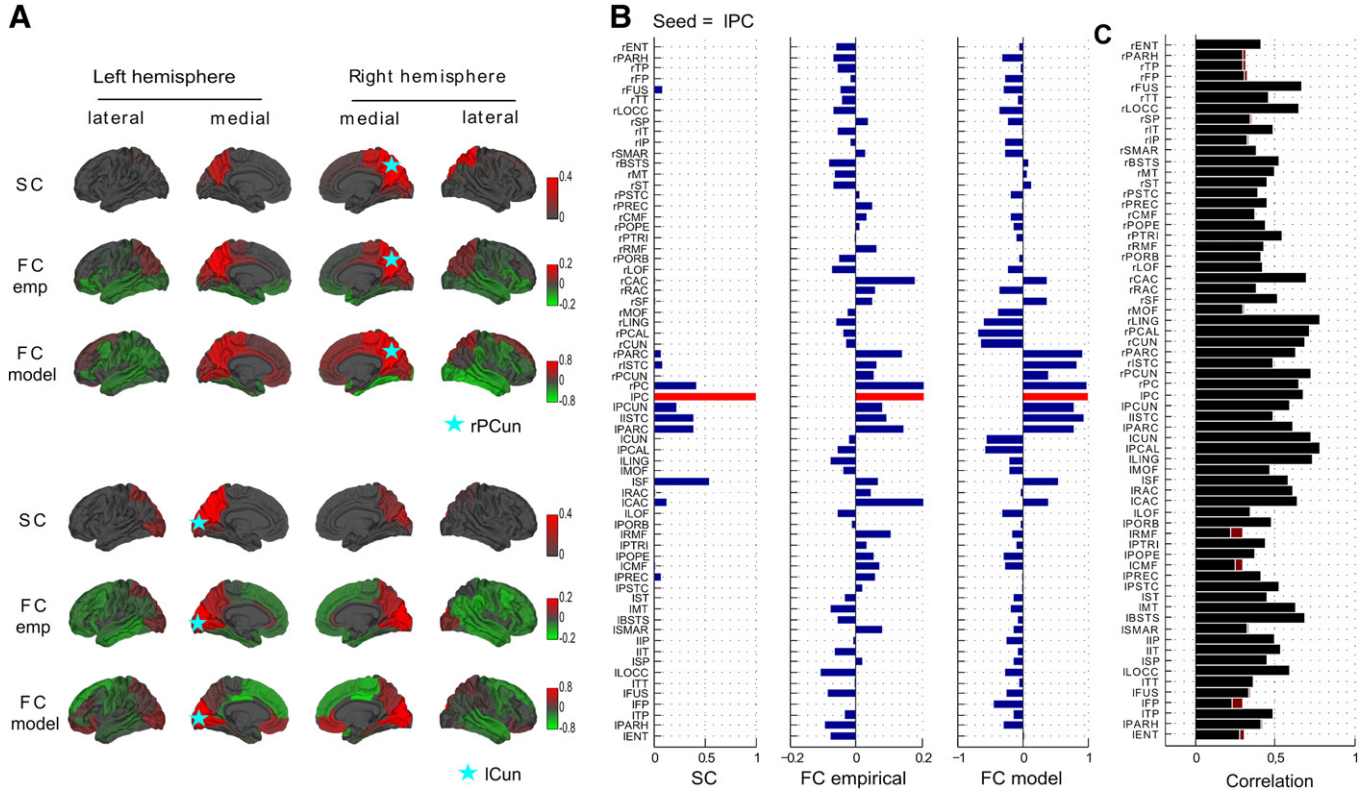

Fig. 7. Comparison between SC, empirical and simulated FC for the working point $(\langle\tau\rangle, k) = (11, 18)$. A, Representation on the cortical surface of the SC (top), empirical (middle) and simulated FC (bottom) maps, for the seeds rPCun (above) and lCUN (below) (seed location indicated by a light blue star). B, SC, empirical and simulated FC for the seed lPC. C, Pearson correlation between empirical and simulated FC for each individual seed. This demonstrates that the model reproduces many details of the empirical FC.

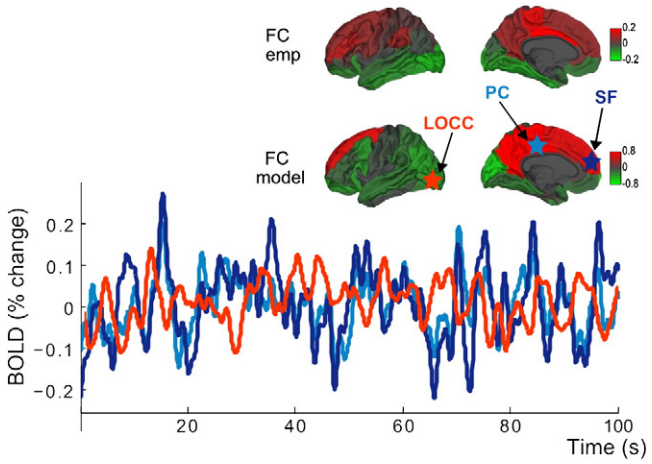

Fig. 8. Correlation between different regions for the working point $(\langle\tau\rangle, k) = (11, 18)$. (Top) Representation on the cortical surface of the empirical and the simulated FC map of the left posterior cingulate (lPC). (Bottom) Simulated BOLD signal for 3 seeds (lPC, light blue; lSF, dark blue; and lLOCC, orange). Both in the empirical and in the simulated data, the FC between lPC and lSF is positive, while their FC with lLOCC is negative.

of the macaque's anatomical brain connectivity (Kötter and Wanke, 2005), a downsampled human SC and a two-dimensional reduced model for the node dynamics including damped alpha oscillations at the local level, slow fluctuations were believed to be induced by noise. This noise led to excursions of neural activity in the vicinity of the stable equilibrium state of the brain network, inducing patterns of alpha waves across the brain network. In Honey et al. (2009), using the high-resolution human SC and a neural mass model at the local level, a similar performance in the comparison with empirical FC as with our model was obtained, but no theoretical explanation for the nature of slow fluctuations was presented. In Deco et al. (2009), Wilson–Cowan units were used at the local level with the CoCoMac connectivity, and the model exhibited similar sustained oscillatory behavior as described here. The network was divided *a priori* into two node communities using a modularity algorithm. What was found was that the synchrony levels of these communities fluctuated in an anti-correlated way under the influence of noise, reproducing experimental observations (Fox et al., 2005). Without the availability of empirical FC for the macaque, the latter model could not go deeper in the analysis, and also did not really address the question of how the BOLD of local nodes gets correlated. Therefore, the goal of the present study was to address all these questions in more detail, using the same dynamical scenario. In the model of Honey et al. (2009), the complex node model did not allow for a good understanding of the origin of the global dynamics. In the other models, either damped oscillations (Ghosh et al., 2008a, 2008b; Knock et al., 2009) or sustained oscillations like here (Deco et al., 2009) were hypothesized at the local level and, even if the dynamics might be mainly linear in the first case, the dynamics was intrinsically nonlinear in the latter. However, in all cases, connectivity, delays and noise were found to be important to reproduce features of the empirical FC, and among them RSNs. For the present model, we find that noise is not necessary to create slow resting-state fluctuations. However, this result does not contradict the results in Deco et al. (2009) as noise was found to play a role in the interaction between clusters, a question that does not overlap with our study.

This study suggests several lines of future research. Although the situation considered here remains too complicated for an analytical treatment, our results predict that the network dynamical behavior we have described could be the origin of fluctuation patterns observed in the BOLD signal during rest. These results emphasize the need for a deeper understanding of the dynamics of phase oscillator networks for complex networks, such as those encountered in the brain. Beyond understanding cluster formation and the emergence of correlations in the slow node dynamics inside clusters, the way these clusters interact and how correlations or anti-correlations emerge between clusters remain unknown. Addressing these questions in future research may help comprehend the organization of neural dynamics at the brain level.

At a broader level, existing models of resting-state activity have considered quite different model dynamics at the local level but, despite their differences, they have shown a degree of agreement with experimental data. This suggests an important role of SC in the generation of FC. As an example, the DMN is known to represent a highly and densely connected subnetwork within the cortex (Hagmann et al., 2008; Honey et al., 2009). However, as we show here, the simulated FC is *a priori* the product of the interplay between SC and the local dynamics. Therefore, improving human connectome data will definitely bring progress to this research field. In future studies, it will also be important to go beyond the BOLD signal in the comparison with experimental data, in the direction of reproducing the more recent experimental findings at the neural activity level (Leopold et al., 2003; Shmuel and Leopold, 2008; Nir et al., 2008; He et al., 2008; Miller et al., 2009; Schölvinck et al., 2010), where neural activity markers of RSNs have begun to be unveiled (Jerbi et al., 2010). In doing so, we will better understand the relationship between spontaneous activity at the local and at the global brain levels.

Acknowledgments

G.D. and E.H. were supported by the European Community's Seventh Framework Program (FP7/2007-2013) grant HEALTH F2 2008 200728, the CONSOLIDER-INGENIO 2010 Programme CSD2007-00012 and the "La Marató" Foundation. J.C. was supported by the Portuguese Foundation for Science and Technology (FCT-POCI 2010) and the European Social Fund (ESF) grant SFRH/BD/36730/2007. O.S. was supported by the JS McDonnell Foundation. We thank Patric Hagmann for the human structural connectivity matrix and Ernest Montbrió for useful discussions on the Kuramoto model. This paper is dedicated to the memory of our friend and colleague, Prof. Rolf Kötter (1961–2010).

Appendix A. Supplementary data

Supplementary data to this article can be found online at doi:10.1016/j.neuroimage.2011.04.010.

References

Acebrón, J.A., Bonilla, L.L., Pérez Vicente, C.J., Ritort, F., Spigler, R., 2005. The Kuramoto model: a simple paradigm for synchronization phenomena. Rev. Mod. Phys. 77, 137–185.
Bartos, M., Vida, I., Jonas, P., 2007. Synaptic mechanisms of synchronized gamma oscillations in inhibitory interneuron networks. Nat. Rev. Neurosci. 8, 45–56.
Beckmann, C.F., DeLuca, M., Devlin, J.T., Smith, S.M., 2005. Investigations into resting-state connectivity using independent component analysis. Philos. Trans. R. Soc. Lond. B 360, 1001–1013.
Biswal, B.B., Yetkin, F.Z., Haughton, V.M., Hyde, J.S., 1995. Functional connectivity in the motor cortex of resting human brain using echo-planar MRI. Magn. Res. Med. 34, 537–541.
Borgers, C., Kopell, N., 2003. Synchronization in networks of excitatory and inhibitory neurons with sparse, random connectivity. Neural Comput. 15, 509–538.
Brunel, N., 2000. Dynamics of sparsely connected networks of excitatory and inhibitory spiking neurons. J. Comput. Neurosci. 8, 183–208.
Brunel, N., Wang, X.-J., 2003. What determines the frequency of fast network oscillations with irregular neural discharges? I. Synaptic dynamics and excitation-inhibition balance. J. Neurophysiol. 90, 415–430.
Bullmore, E., Sporns, O., 2009. Complex brain networks: graph theoretical analysis of structural and functional systems. Nat. Rev. Neurosci. 103, 186–198.
Damoiseaux, J.S., Rombouts, S.A.R.B., Barkhof, F., Scheltens, P., Stam, C.J., Smith, S.M., Beckmann, C.F., 2006. Consistent resting-state networks across healthy subjects. Proc. Natl. Acad. Sci. U. S. A. 103, 13848–13853.
Deco, G., Jirsa, V., McIntosh, A.R., Sporns, O., Kötter, R., 2009. Key role of coupling, delay and noise in resting brain fluctuations. Proc. Natl. Acad. Sci. U. S. A. 106, 10302–10307.

Fox, M.D., Raichle, M.E., 2007. Spontaneous fluctuations in brain activity observed with functional magnetic resonance imaging. Nat. Rev. Neurosci. 8, 700–711.
Fox, M.D., Snyder, A., Vincent, J., Corbetta, M., Van Essen, D., Raichle, M., 2005. The human brain is intrinsically organized into dynamic, anticorrelated functional networks. Proc. Natl. Acad. Sci. U. S. A. 102, 9673–9678.
Fox, M.D., Zhang, D., Snyder, A.Z., Raichle, M.E., 2009. The global signal and observed anticorrelated resting state brain networks. J. Neurophysiol. 101, 3270–3283.
Friston, K., Harrison, L., Penny, W., 2003. Dynamic causal modelling. Neuroimage 19, 1273–1302.
Friston, K.J., Li, B., Daunizeau, J., Stephan, K.E., 2010. Network discovery with DCM. NeuroImage 56, 1202–1221.
Ghosh, A., Rho, Y., McIntosh, A.R., Kotter, R., Jirsa, V.K., 2008a. Noise during rest enables the exploration of the brain's dynamic repertoire. PLoS Comput. Biol. 4, e1000196.
Ghosh, A., Rho, Y., McIntosh, A.R., Kotter, R., Jirsa, V.K., 2008b. Cortical network dynamics with time delays reveals functional connectivity in the resting brain. Cogn. Neurodyn. 2, 115–120.
Greicius, M., Krasnow, B., Reiss, A., Menon, V., 2003. Functional connectivity in the resting brain: a network analysis of the default mode hypothesis. Proc. Natl. Acad. Sci. U. S. A. 100, 253–258.
Gusnard, D., Raichle, M., 2001. Searching for a baseline: functional imaging and the resting human brain. Nat. Rev. Neurosci. 2, 685–694.
Hagmann, P., Kurant, M., Gigandet, X., Thiran, P., Wedeen, V.J., Meuli, R., Thiran, J.-P., 2007. Mapping human whole-brain structural networks with diffusion MRI. PLoS One 2, e597.
Hagmann, P., Cammoun, L., Gigandet, X., Meuli, R., Honey, C.J., Wedeen, V.J., Sporns, O., 2008. Mapping the structural core of human cerebral cortex. PLoS Biol. 6, e159.
He, B.J., Snyder, A.Z., Zemple, J.M., Smyth, M.D., Raichle, M.E., 2008. Electrophysiological correlates of the brain's intrinsic large-scale functional architecture. Proc. Natl. Acad. Sci. U. S. A. 105, 16039–16044.
Honey, C.J., Sporns, O., Cammoun, L., Gigandet, X., Thiran, J.P., Meuli, R., Hagmann, P., 2009. Predicting human resting-state functional connectivity from structural connectivity. Proc. Natl. Acad. Sci. U. S. A. 106, 2035–2040.
Jerbi, K., Vidal, J.R., Ossandon, T., Dalal, S.S., Jung, J., Hoffmann, D., Minotti, L., Bertrand, O., Kahane, P., Lachaux, J.-P., 2010. Exploring the electrophysiological correlates of the default-mode network with intracerebral EEG. Front. Syst. Neurosci. 4 article 27.
Kilner, J.M., Mattout, J., Henson, R., Friston, K.J., 2005. Hemodynamic correlates of EEG: a heuristic. NeuroImage 28, 280–286.
Knock, S.A., McIntosh, A.R., Sporns, O., Kötter, R., Hagmann, P., Jirsa, V.K., 2009. The effects of physiologically plausible connectivity structure on local and global dynamics in large scale brain models. J. Neurosci. Methods 183, 86–94.
Kötter, R., 2004. Online retrieval, processing, and visualization of primate connectivity data from the CoCoMac database. Neuroinformatics 2, 127–144.
Kötter, R., Wanke, E., 2005. Mapping brains without coordinates. Philos. Trans. R. Soc. Lond. B 360, 751–766.
Kuramoto, Y., 1984. Chemical Oscillations, Waves, and Turbulence. Springer-Verlag, Berlin.
Lee, W.S., Ott, E., Antonsen, T.M., 2009. Large coupled oscillator systems with heterogeneous interaction delays. Phys. Rev. Lett. 103, 044101.
Leopold, D.A., Murayama, Y., Logothetis, N.K., 2003. Very slow activity fluctuations in monkey visual cortex: implications for functional brain imaging. Cereb. Cortex 13, 422–433.
Mantini, D., Perrucci, M., Del Gratta, C., Romani, G., Corbetta, M., 2007. Electrophysiological signatures of resting state networks in the human brain. Proc. Natl. Acad. Sci. U. S. A. 104, 13170–13175.
Mattia, M., Del Giudice, P., 2002. Population dynamics of interacting spiking neurons. Phys. Rev. E 66, 051917.
Miller, K.J., Weaver, K.E., Ojemann, J.G., 2009. Direct electrophysiological measurement of human default network areas. Proc. Natl. Acad. Sci. U. S. A. 106, 12174–12177.
Nir, Y., Mukamel, R., Dinstein, I., Privman, E., Harel, M., Fisch, L., Gelbard-Sagiv, H., Kipervasser, S., Andelman, F., Neufeld, M.Y., Kramer, U., Arieli, A., Fried, I., Malach, R., 2008. Interhemispheric correlations of slow spontaneous neuronal fluctuations revealed in human sensory cortex. Nat. Neurosci. 11, 1100–1108.
Platen, E., 1999. An introduction to numerical methods for stochastic differential equations. Acta Num. 197–246.
Popovych, O.V., Maistrenko, Y.L., Tass, P.A., 2005. Phase chaos in coupled oscillators. Phys. Rev. E 71, 065201.
Raichle, M., Mintun, M., 2006. Brain work and brain imaging. Annu. Rev. Neurosci. 29, 449–476.
Rosa, M.J., Daunizeau, J., Friston, K.J., 2010. EEG-fMRI integration: a critical review of biophysical modelling and data analysis approaches. J. Integr. Neurosci. 9 (4), 453–476.
Schölvinck, M.L., Maier, A., Ye, F.Q., Duyn, J.H., Leopold, D.A., 2010. Neural basis of global resting-state fMRI activity. Proc. Natl. Acad. Sci. U. S. A. 107, 10238–10243.
Shanahan, M., 2010. Metastable chimera states in community-structured oscillator networks. Chaos 20, 013108.
Shmuel, A., Leopold, D.A., 2008. Neuronal correlates of spontaneous fluctuations in fMRI signals in monkey visual cortex: implications for functional connectivity at rest. Hum. Brain Mapp. 29, 751–761.
Vincent, J., Patel, G., Fox, M., Snyder, A., Baker, J., Van Essen, D., Zempel, J., Snyder, L., Corbetta, M., Raichle, M., 2007. Intrinsic functional architecture in the anaesthetized monkey brain. Nature 447, 83–86.
Wilson, H.R., Cowan, J.D., 1972. Excitatory and inhibitory interactions in localized populations of model neurons. Biophys. J. 12, 1–23.
Yeung, M.K.S., Strogatz, S.H., 1999. Time delay in the Kuramoto model of coupled oscillators. Phys. Rev. Lett. 82, 648–651.

Role of Local Network Oscillations in Resting-State Functional Connectivity

Joana Cabral, Etienne Hugues, Olaf Sporns, Gustavo Deco

Supplementary Material

Supplementary Table 1. Names and abbreviations of the brain regions considered in the human connectome (in alphabetical order).

Abbreviation	Brain region
BSTS	Bank of the superior temporal sulcus
CAC	Caudal anterior cingulate cortex
CMF	Caudal middle frontal cortex
CUN	Cuneus
ENT	Entorhinal cortex
FP	Frontal pole
FUS	Fusiform gyrus
IP	Inferior parietal cortex
ISTC	Isthmus of the cingulate cortex
IT	Inferior temporal cortex
LING	Lingual gyrus
LOCC	Lateral occipital cortex
LOF	Lateral orbitofrontal cortex
MOF	Medial orbitofrontal cortex
MT	Middle temporal cortex
PARC	Paracentral lobule
PARH	Parahippocampal cortex
PC	Posterior cingulate cortex
PCAL	Pericalcarine cortex
PCUN	Precuneus
POPE	Pars opercularis
PORB	Pars orbitalis
PREC	Precentral gyrus
PSTC	Postcentral gyrus
PTRI	Pars triangularis
RAC	Rostral anterior cingulate cortex
RMF	Rostral middle frontal cortex
SF	Superior frontal cortex
SMAR	Supramarginal gyrus
SP	Superior parietal cortex
ST	Superior temporal cortex
TP	Temporal pole
TT	Transverse temporal cortex.

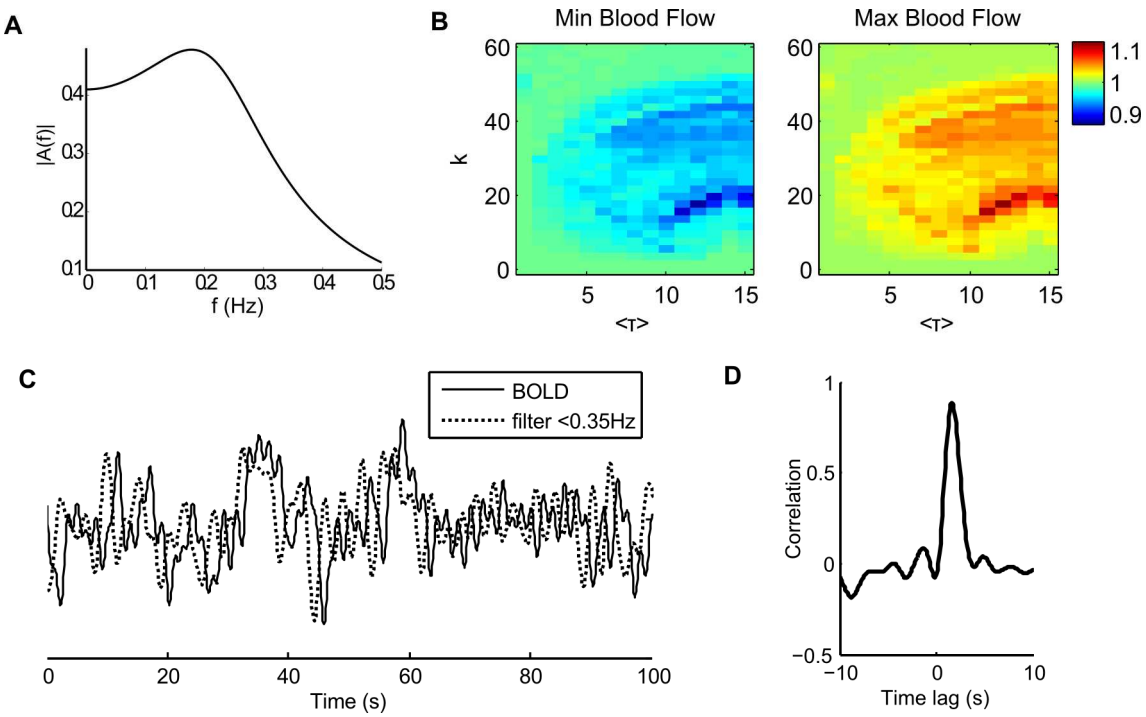

Supplementary Figure 1. Characteristics of the BOLD signal from the Balloon-Windkessel model. ***A***, Amplitude of the linear filter in the Balloon-Windkessel model as a function of frequency. **B**, Diagrams representing the minimum value (left) and the maximum value (right) of the blood flow as a function of the mean delay, $<\tau>$, and the coupling strength, k. This was obtained considering r_0 =1, i.e., simulated rates fluctuate between -1 and 1. The blood flow fluctuates 15% at most. This means that for the value of r_0 we have chosen, the Balloon model is behaving essentially linearly, proving that the patterns we observe at the BOLD level come essentially from the network dynamics. ***C***, Comparison between the BOLD signal (solid line) and the corresponding low-pass filtered neural activity with a cut-off frequency of 0.35Hz (dotted line). ***D***, Cross-correlation between the two signals; the peak around 1.6 s (correlation coefficient = 0.88) corresponds to the lag of the hemodynamic response.

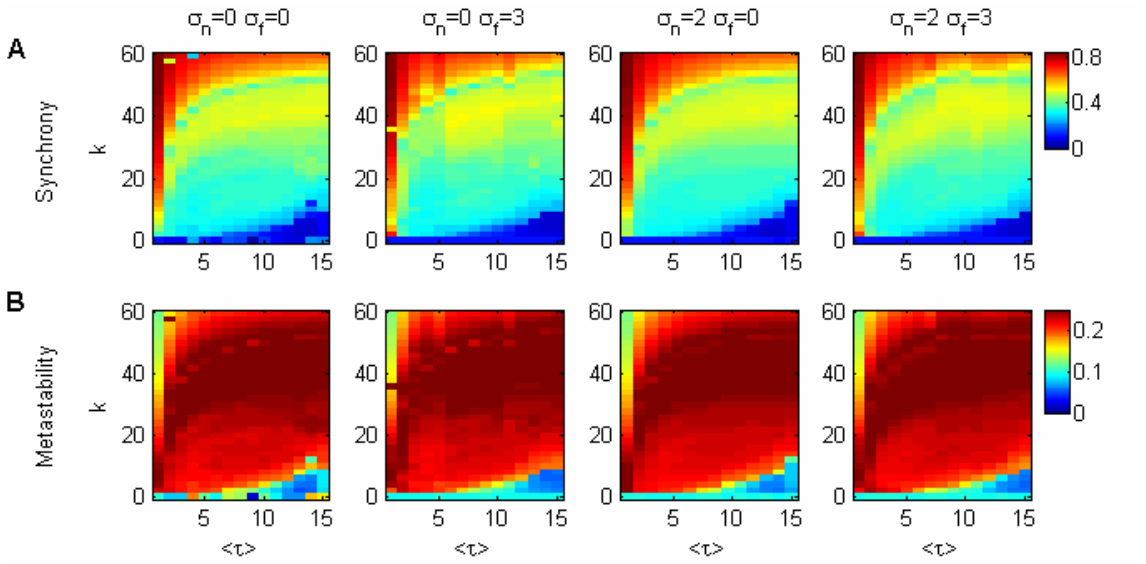

Supplementary Figure 2. Global dynamics in the mean delay and global coupling parameter space for (σ_n,σ_f) = (0,0), (0,3), (2,0) and (2,3). ***A***, Global level of synchrony measured as the mean of the order parameter $R(t)$. ***B***, Global level of metastability, given by the standard deviation σ_R of the order parameter. We observe that the dynamics at the global level is only slightly affected by the dispersion of intrinsic frequencies and the noise.

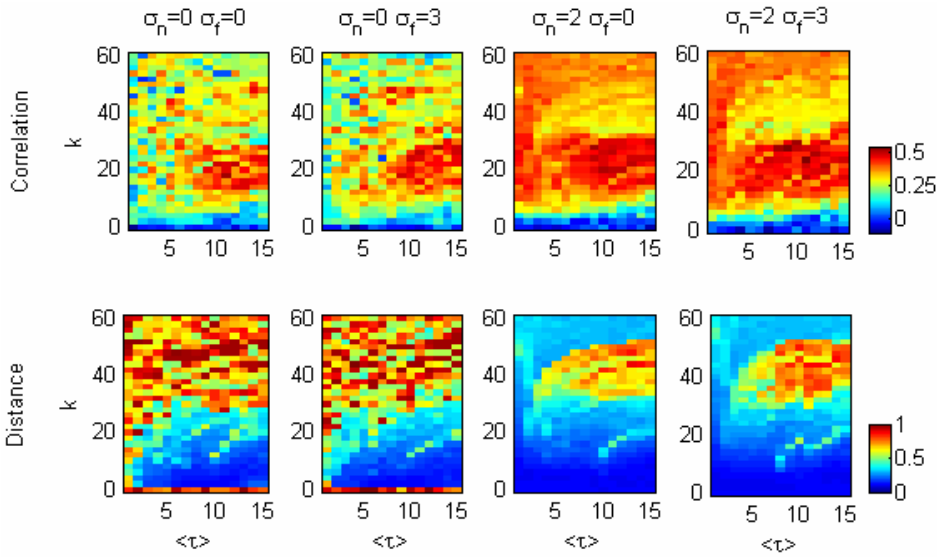

Supplementary Figure 3. Behavior of the simulated FC in the parameter space. Pearson correlation (top) and distance (bottom) between the empirical and the simulated FC in the (<τ>,k) parameter space for (σ_n,σ_f) = (0,0), (0,3), (2,0) and (2,3). Only connected pairs of regions are considered. These results reveal that the region of best agreement is the same with or without noise and frequency dispersion (maximal correlation and minimal distance or error), proving in this way the robustness of the dynamics in realistic conditions. Moreover, this region coincides with delays from 8 to 15 ms, corresponding to axonal conduction velocities from 4 to 8 m/s, which is in the range of velocities reported in literature.

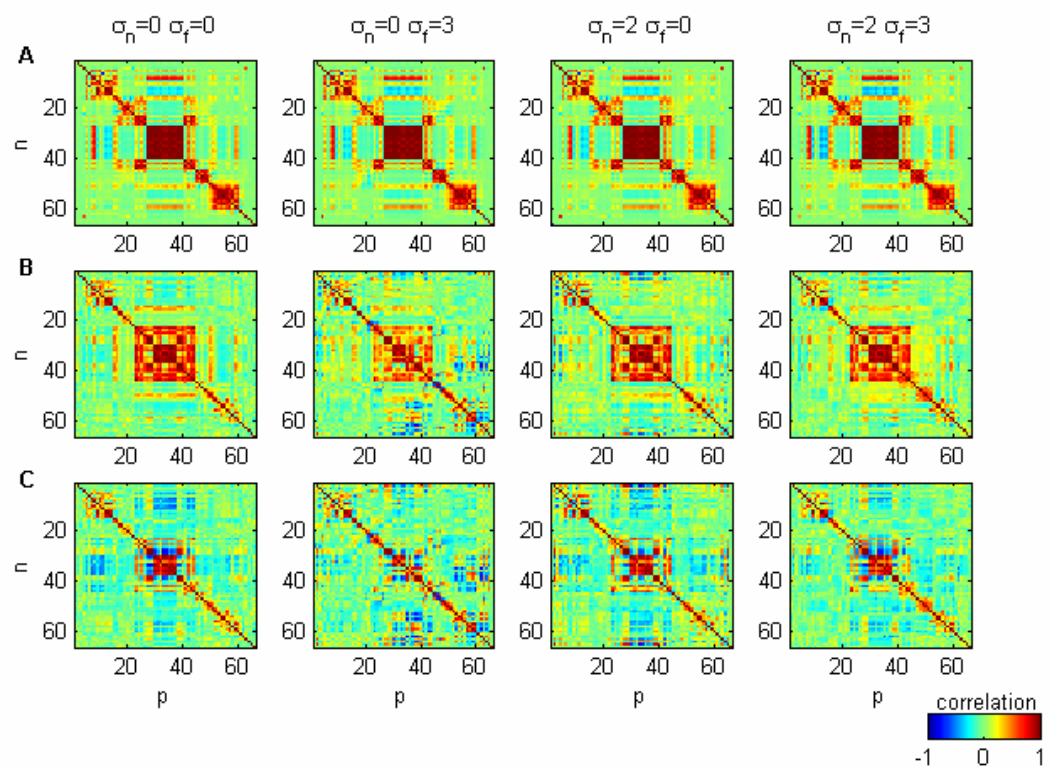

Supplementary Figure 4. Correlation matrices of the simulated neural activity (**A**), the simulated BOLD activity (**B**) and after the removal of the global signal (**C**) for the selected working point (<τ>,k) = (11,18), for different noise and frequency dispersion levels as (σ_n,σ_f) = (0,0), (0,3), (2,0) and (2,3) (from left to right).

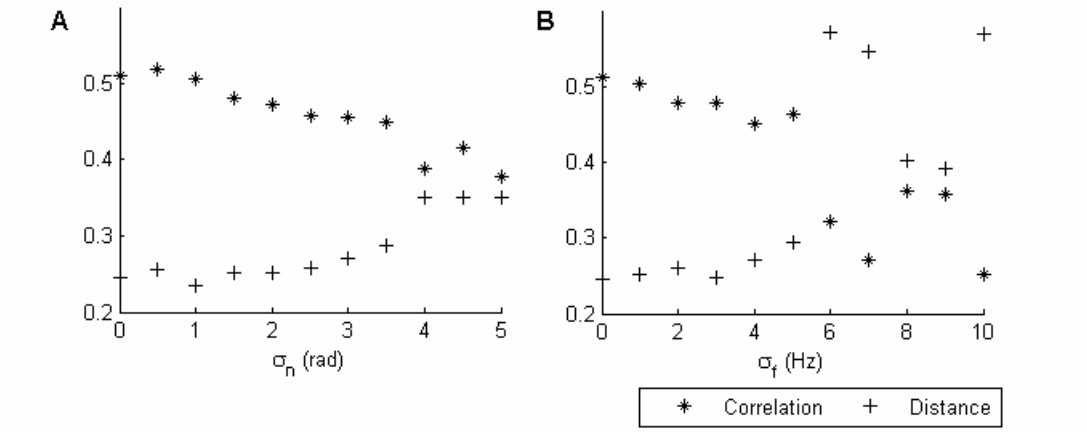

Supplementary Figure 5. Robustness of model results with respect to (***A***) noise standard deviation σ_n and (***B***) frequency distribution standard deviation σ_f for the chosen working point (<τ>,*k*) = (11,18). (*****) Pearson correlation and (+) distance between the simulated and the empirical FC, for anatomically connected pairs of regions. In the biologically realistic range of frequency dispersion ($\sigma_f \leq 5$ Hz), and noise ($\sigma_n \leq 3$ rad), the performance of the model is essentially unchanged.

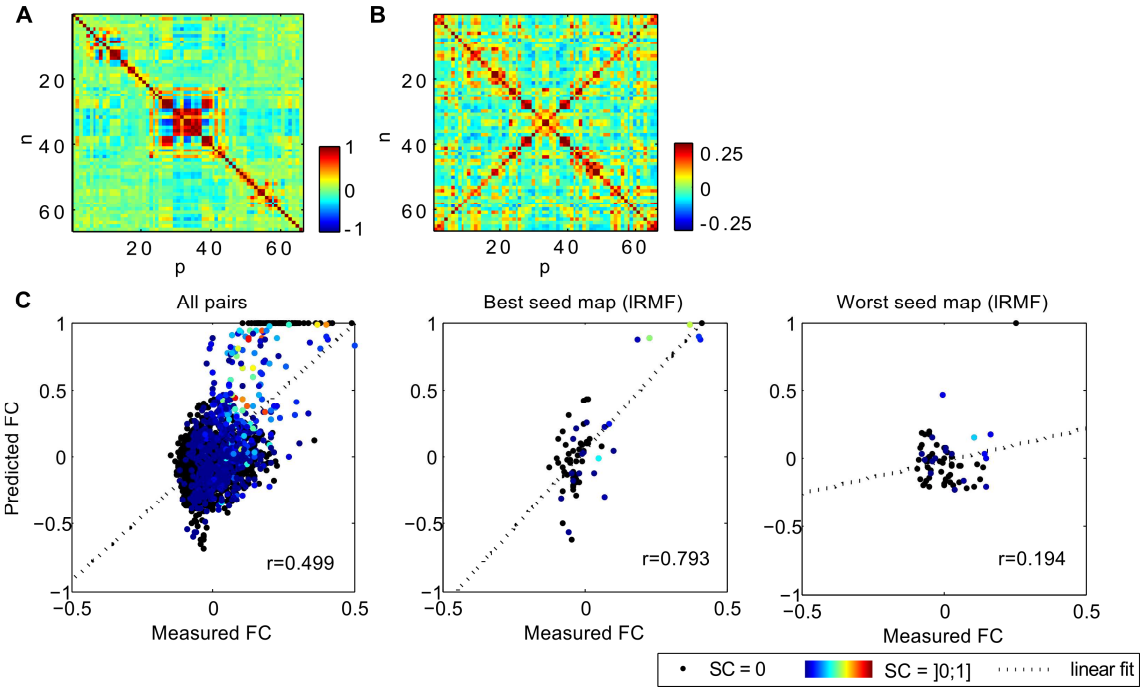

Supplementary Figure 6. Comparison between the simulated and the empirical FC for the chosen working point and with noise (σ_n = 1.25). ***A***, Simulated FC matrix (after regression of the global signal). ***B***, Empirical FC matrix. The model results reproduce a number of details of the empirical data. Note, however, the lack of positive simulated FC between contralateral homologous regions (along the anti-diagonal) outside of the matrix center, which are naturally present in the empirical FC. This deficiency is attributable to the SC where connections between these areas are absent (See Figure 1B). Indeed, due to shortcomings of DSI and tractography to measure the SC, some small fiber tracts and interhemispheric connections toward lateral cortices may be underrepresented given the limited resolution and complexity of the anatomy in the centrum semiovale (Hagmann et al., 2008). ***C***, Scatter plots of predicted versus measured FC for all pairs of seeds (left), for the best seed only (center) and for the worst seed (right). Red Black dots correspond to correlations between disconnected pairs. Correlations between structurally connected pairs are coloured according to SC strength (which was normalized to 1). Linear regressions (dashed lines) were calculated considering connected and disconnected pairs altogether.